Scaling of the surface vasculature on the human placenta

A. S. Leonard,[1] J. Lee,[1] D. Schubert,[1] L. A. Croen,[2] M. D. Fallin,[3] C. J. Newschaffer,[4] C. K. Walker,[5] C. M. Salafia,[6]
S. P. Morgan,[1] and D. D. Vvedensky[1]

[1]*The Blackett Laboratory, Imperial College London, London SW7 2AZ, United Kingdom*
[2]*Division of Research, Kaiser Permanente Northern California, Oakland, California 94612, USA*
[3]*Department of Epidemiology and Department of Biostatistics, Johns Hopkins, Bloomberg School of Public Health,*
Johns Hopkins University Baltimore, Maryland 21205, USA
[4]*Department of Epidemiology and Biostatistics, Drexel School of Public Health, Drexel University 1505 Race Street, Mail Stop 1033,*
Philadelphia, Pennsylvania 19102, USA
[5]*Lawrence J. Ellison Ambulatory Care Center, Obstetrics and Gynecology Clinic, University of California–Davis,*
Sacramento, California 95817, USA
[6]*Placental Analytics, LLC, 187 Overlook Circle, New Rochelle, New York 10804, USA*

The networks of veins and arteries on the chorionic plate of the human placenta are analyzed in terms of Voronoi cells derived from these networks. Two groups of placentas from the United States are studied: a population cohort with no prescreening, and a cohort from newborns with an elevated risk of developing autistic spectrum disorder. Scaled distributions of the Voronoi cell areas in the two cohorts collapse onto a single distribution, indicating common mechanisms for the formation of the complete vasculatures, but which have different levels of activity in the two cohorts.

The human placenta is the interface between mother and fetus, providing the sole source of nutrients to the fetus, removing waste, and establishing a barrier against antigen attack [1,2]. Placental measures, such as weight, shape, thickness, and umbilical cord site are known [3,4] to affect birth outcomes, as are genetic and environmental factors. The placenta has an active role in the fetal endocrine system, providing controlling factors in fetal development [5]. Barker's hypothesis [6–8] links fetal development not just to fetal and childhood health but, by relating adult mortality, stroke, heart disease, and chronic bronchitis to prenatal factors and maternal health, to adult health as well.

The exchange of material between mother and fetus is facilitated by the vasculature—the network of veins and arteries within the placenta. The vascular system emanates from arteries and veins that extend from the fetus to the placenta through the umbilical cord, which usually attaches near the center of a placenta. Branching begins at the cord insertion, initially on the chorionic plate, before diving into the interior of the placenta, where there is further branching. The exchange of respiratory gases (mainly O_2 and CO_2), nutrients, and waste occurs through the finest vessels (capillaries within the terminal villi).

Here, we analyze the vasculatures of placentas from two cohorts from the United States: the National Children's Study (NCS) [9], which had no prescreening and is, therefore, a population cohort, and the Early Autism Risk Longitudinal Investigation (EARLI) [10], which selects newborns with an elevated risk of developing autistic spectrum disorder. The EARLI cohort is from a network of research sites that enrolled mothers of children with autism at the start of another pregnancy and documents the development of the newborns, so far covering the first three years. EARLI examines possible environmental risk factors for autism and whether there is any interplay between such factors and genetic susceptibility.

Our analysis is based on a partition of the chorionic plate area of each placenta into contiguous polygonal regions, called Voronoi cells [11]—one for each blood vessel. This construction affords an analysis that has proven useful in other cellular systems [12–14]. In particular, when expressed in terms of areas scaled by their average, the distributions of Voronoi cell areas in the two cohorts collapse onto a single distribution. This indicates that the overall mechanism for the formation of the vasculature is the same in these cohorts, but is less active in the EARLI cohort, yielding a lower branching density (Table I).

Table I compares several basic measures of the placentas from the two cohorts. The average areas and perimeters are virtually identical. However, there is a substantial difference in the numbers of vertices, which are bifurcation points of the vasculature. Thus, the NCS placentas have shorter blood vessels with more branching, so more extensive coverage of the chorionic plate than EARLI placentas. A comprehensive analysis of these placentas and their vasculatures will be presented elsewhere.

The passage from a vascular network to its Voronoi representation is illustrated in Fig. 1. Figure 1(a) shows a hand-tracing [15] of the arteries on a digital image of a placenta. Starting from the umbilical cord (the origin) and moving along the edges (blood vessels), a vertex at the beginning of an edge is called the parent of the vertex at the end of that edge, and the vertex at the end of an edge is called a child of the parent vertex. Vertices are assigned generation numbers g to indicate their position within the network. The origin has $g = 1$, with g increasing by 1 from parent to child. An edge of generation g connects vertices of generations g and $g + 1$.

The Voronoi construction is based on seeds placed at the midpoint of each blood vessel [Fig. 1(b)], which is approximated by the centers of straight lines connecting the

TABLE I. Basic measures of the N placentas used from the NCS and EARLI cohorts. A is their average area, P their average perimeter, and n_v and n_a average numbers of vertices in their venous and arterial networks, respectively. Significance of the differences is indicated by multiples n_σ of the standard error.

	NCS	EARLI	n_σ
N	201	75	
A (cm^2)	273	271	0.33
P (cm)	64.7	64.8	0.07
n_v	97.0	69.3	7.48
n_a	98.0	68.4	6.99

parent and child vertices of the vessel. Figure 1(c) shows the resulting Voronoi cells, whose sides are perpendicular bisectors of the lines connecting a seed to its neighboring seeds. Points in the enclosed polygon are closer to that seed than to any other. The Voronoi cell area therefore provides an estimate of the region served by the blood vessel. Two types of cell are obtained: "core" cells, which are contained entirely within the placenta, and "boundary" cells, which are truncated by the edge of the placenta. Our analysis is based on core cells. Figure 1(d) shows the Voronoi cells color-coded by generation.

We have also examined Voronoi distributions derived from seeds of other network components. Using the vertices produces results similar to those reported here. A somewhat different construction is based on *entire* blood vessel segments. The resulting Voronoi cells also show scaling, but only when the cell area is replaced by the cell volume that includes the thickness of the placenta over the cell area. Taken together, these results indicate that scaling is an intrinsic part of placental vasculature.

Histograms of Voronoi cell areas are shown in Fig. 2 for veins and arteries in placentas from the NCS and EARLI cohorts. These histograms were obtained from the cell areas within each placenta, which were put into uniform bins whose width was chosen by balancing a discernible distribution against the smoothness of that distribution.

Several similarities and differences are apparent in Fig. 2. The NCS data show a greater maximum at small areas, with
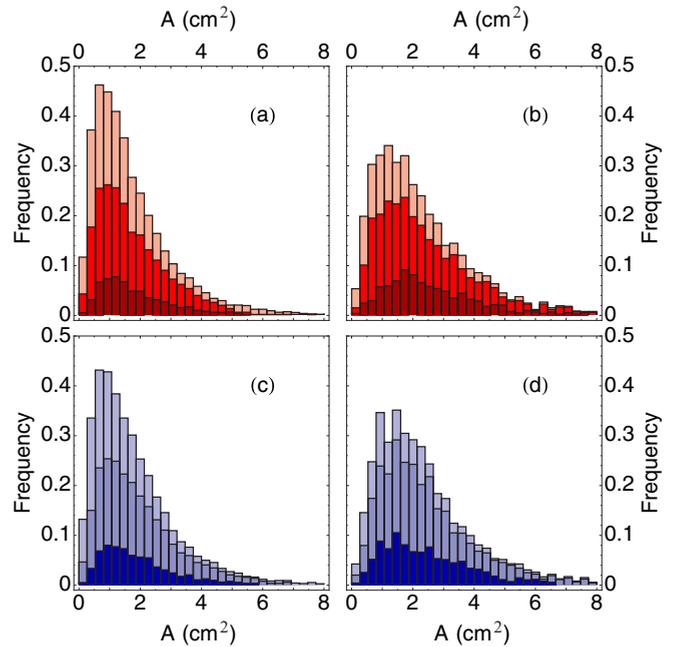
FIG. 2. Histograms of core Voronoi cell areas for (a) NCS arteries (b) EARLI arteries, (c) NCS veins, and (d) EARLI veins. The cumulative contributions for the first three and first six generations are indicated by darker and lighter shading, respectively, in each panel.

a more rapid decrease at larger areas than the EARLI cohort. The two cohorts have approximately equal average chorionic plate area (Table I), so the differences in Fig. 2 are due to the differences in the numbers of veins and arteries between the two cohorts. On average larger regions of placentas in the EARLI cohort are served by the blood vessels than those in the NCS cohort.

Placentas from the NCS and EARLI cohorts are shown in Fig. 3. The number, sizes, and spatial arrangements of the Voronoi cells in the two cohorts are discernibly different. The placentas in the NCS cohort [Figs. 3(a) and 3(b)] have ∼70 core cells, with several clusters of small cells. Those from EARLI [Figs. 3(c) and 3(d)] have ∼50 core cells, with fewer small cells. These are consistent with the histograms in Fig. 2.

The other striking feature in the histograms is that the distributions of venous and arterial Voronoi areas are essentially
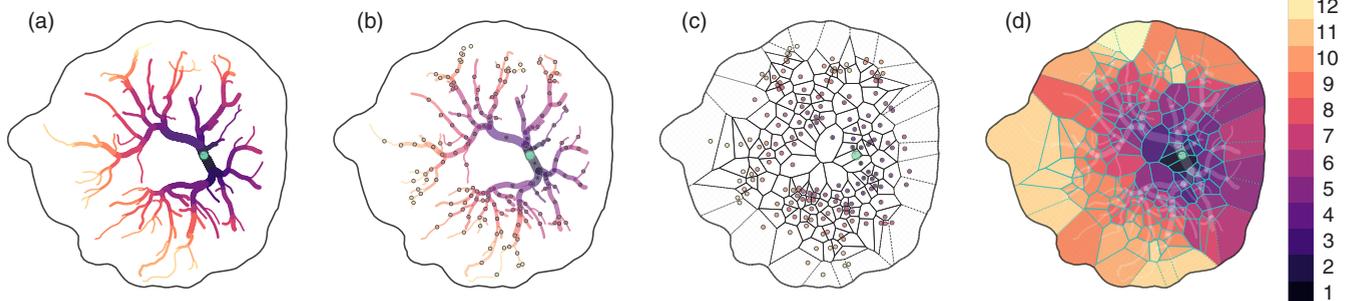
FIG. 1. (a) Digital image of the chorionic plate of a placenta from the NCS cohort with the hand-tracing of the arteries and their thicknesses. The regular shape and near-central umbilical cord insertion (indicated by the blue circle) are expected of a "normal" placenta. (b) Representation of each blood vessel as a seed at its midpoint, indicated by filled circles. (c) Voronoi cells obtained from the seeds in (b). (d) Generations of Voronoi cells according to the adjacent color bar. The same color coding for generations is used in (a) and (b).
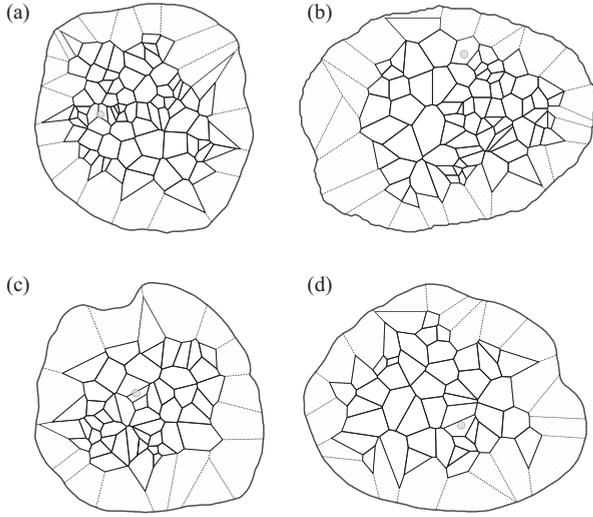
FIG. 3. Voronoi constructions of placentas from the [(a),(b)] NCS and [(c),(d)] EARLI cohorts. Core and boundary cells are shown as unshaded and shaded regions, respectively. The umbilical cord insertions are indicated by light blue circles.

the same for each cohort. This similarity is not altogether surprising, as the average numbers of vertices in the venous and arterial networks in the two cohorts are essentially the same (Table I).

An alternative presentation of the data in Fig. 2 is a scaling plot, in which the density $P(A)$ of Voronoi cells with area A is plotted against the Voronoi cell area divided by the average cell area $\langle A \rangle$ of each placenta to form a new histogram. Such plots [16] enable placentas within and between cohorts to be compared directly. Scaled histograms are shown in Fig. 4 with bin widths chosen to optimize the statistics for comparisons to particular distributions. All four data sets in Fig. 2 "collapse"
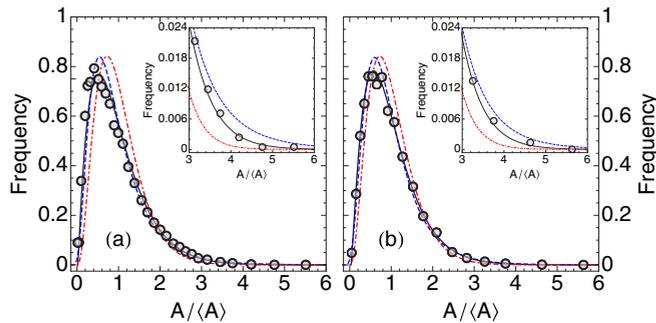
FIG. 4. Scaling plots of the data in Fig. 2 for the (a) NCS and (b) EARLI cohorts. The similarity of the two best-fit distributions (Table II) points to a collapse of all data into a single scaling function. Bin widths in (0,3] have comparable numbers of data points, while those in (3,6] each have at least 30 data points. Comparisons are made between the data points and the best fit gamma (solid black curve), best fit lognormal (broken blue curve), and random gamma (dot-dashed red curve) distributions. The insets show magnifications for the fits to the tails of the distributions. See text and Table II for details.

TABLE II. Optimized parameters for the gamma and lognormal distributions in (2) and (3), together with the "exact" results for the random gamma function: $a = 0$, $b = \frac{7}{2}$, and $c = \frac{2}{7}$ [14]. The p values were obtained from the Anderson-Darling test.

		a (location)	b (shape)	c (scale)	p value
	Random	0	3.5	0.29	0.002
NCS	Lognormal	-0.15	0.58	0.97	0.03
	Gamma	0.02	2.10	0.46	0.13
	Random	0	3.5	0.29	0.008
EARLI	Lognormal	-0.20	0.52	1.05	0.03
	Gamma	0.03	2.30	0.42	0.10

onto a single "scaling function" f,

$$P(A) = \frac{1}{\langle A \rangle} f\left(\frac{A}{\langle A \rangle}\right), \tag{1}$$

with normalization $\int_0^\infty f(s)\,ds = 1$ and first moment $\int_0^\infty s f(s)\,ds = 1$. The data collapse of the histograms in Fig. 2 indicates that, despite the difference in the spatial patterns of the Voronoi cells in the two cohorts (Fig. 2), there is a common mechanism for the cumulative formation of the vasculature.

The distributions for different types of Voronoi decompositions [14], and the lognormal distribution in the life sciences [17,18], invites comparisons with the scaling function in Fig. 4. We tested the random gamma, optimized gamma, and the optimized lognormal distributions. The gamma distribution is

$$f(s) = \frac{(s-a)^{b-1}}{c^b \Gamma(b)} \exp\left(-\frac{s-a}{c}\right), \tag{2}$$

where a, b, and c are, respectively, the location, shape, and scale parameters. For two-dimensional Voronoi cells generated from random seeds (a Poisson Voronoi diagram), the cell areas follow a gamma distribution with approximate values [14] $a = 0$, $b = \frac{7}{2}$, and $c = \frac{2}{7}$, although other studies found slightly different values [12]. The lognormal distribution is

$$f(s) = \frac{1}{(s-a)\sqrt{2\pi b^2}} \exp\left\{-\frac{1}{2b^2}\left[\ln\left(\frac{s-a}{c}\right)\right]^2\right\}, \tag{3}$$

where a, b, and c have the same meanings as in (2). The lognormal distribution is obtained for variables that are products of a large number of independent, identically distributed variables. The gamma distribution results for variables that are sums of a large number of independent exponential random variables, that is, variables from the arrival times of a Poisson process.

The random, optimized gamma, and optimized lognormal distributions with the parameters in Table II are compared with the collapsed data in Fig. 4. The p values [19] were determined from the Anderson-Darling test [20], which is a modification of the Kolmogorov-Smirnov test that places more weight on the tails of the distributions. The random distribution produces p values that fail the significance level of 0.05, which can be seen from the inadequacy of the fit to the peak and the profile of the tail. Only the gamma distribution has p values above 0.05, but the lognormal distribution produced p values close to this level. Some of this discrepancy can be attributed to the points near the peak, where the statistical variations are
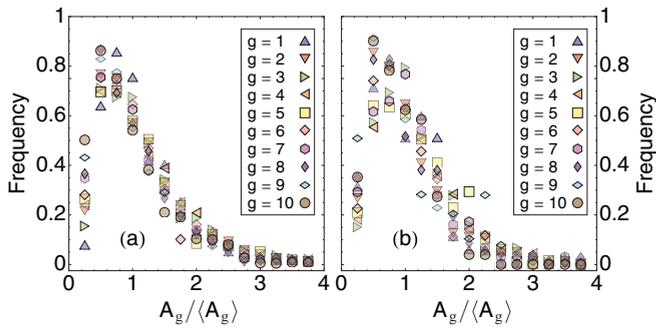
FIG. 5. Scaling plots of Voronoi core cell areas for arteries of the (a) NCS and (b) EARLI chorionic vasculatures resolved according to generation g for the first ten generations. The tighter data collapse for NCS is likely due to the larger number of placentas in that cohort (Table I).

typically the largest, but the profile of the tail favors the gamma distribution.

The vasculature of the human placenta is formed over several stages during pregnancy [21]. The topologies of the measured vascular networks are determined by the process of branching angiogenesis, which is observed during about the first 6 months of pregnancy [21,22]. We expect that during the remaining 3 months, the lengths and widths of vessels within the venous and arterial networks adjust in response to the local environment to produce the vasculatures analyzed here. As the layout of the vasculature changes in the final 3 months of pregnancy, the Voronoi cells at 6 months could alter their sizes and shapes (metric properties), while their generation numbers and the number of cells could remain invariant (topological properties).

The data collapse implied by Fig. 4 shows that the vasculatures of the NCS and EARLI cohorts are characterized by a single scale, the average Voronoi cell area. All of the differences in vascular development are subsumed by this quantity, which suggests common overall formation mechanisms in the two cohorts. The lower branching density in the EARLI placentas (Table I) indicates that this mechanism is less active overall in this cohort, although the reason(s) for this, whether genetic or environmental [23], is inaccessible to a scaling analysis. The poor fit of the random gamma distribution indicates that our seed positions are not random. The examples in Fig. 3 support this by the tendency toward clustering of large cells and small cells. This can be quantified by a two-point correlation function of Voronoi areas.

That the best fit in Fig. 4 is a gamma distribution is not altogether surprising given the prevalence of this distribution in other biological systems generally [24–26], and the analysis of models of vascular networks [27–29] in particular. While the gamma distribution is consistent with branching governed by processes with exponential waiting times, the 3-month adjustment phase could mean that other processes are operative. The key question here is the relationship between the distribution function at around 6 months and that at full term. The simplest such scenario is seen in certain surface growth phenomena [30], where there is an incubation period during which certain features are formed with a particular distribution. Subsequently growth is self-similar, with few additional new features, leaving the distribution function invariant.

Finally, Fig. 5 shows scaling plots for Voronoi cell areas for the arterial networks in the NCS and EARLI cohorts resolved according to generation for the first ten generations. The data collapse for the NCS data suggests that the formation of the vasculature may involve self-organization resulting from interactions between neighboring generations. The corresponding data for the EARLI are more scattered, which may be due to the smaller sample size.

The results presented here can be expanded and generalized in several ways. Examining placentas from others selected for other abnormalities, such as hypertension or diabetes, could strengthen the case for the distribution of Voronoi cells being universal, or require additional factors to be taken into account. Our approach could also be extended to the full three-dimensional vasculature [31]. While not as accessible as the surface vasculature, imaging methods are becoming available [32,33] that reveal the full vasculature of the placenta. Finally, taking a broader view, comparisons between the vasculatures of the placenta and other organs, which are available in mice [34], would provide a direct way of assessing common features and variations in vascular formation.

[1] K. Benirschke and P. Kaufmann, *Pathology of the Human Placenta*, 4th ed. (Springer, New York, 2000).

[2] G. J. Burton and A. L. Fowden, Philos. Trans. R. Soc. London B **370**, 20140066 (2015).

[3] L. H. Sanin, S. R. López, E. T. Olivares, M. C. Terrazas, M. A. R. Silva, and M. L. Carrillo, Biol. Neonate. **80**, 113 (2001).

[4] C. M. Salafia, J. Zhang, R. K. Miller, A. K. Charles, P. Shrout, and W. Sun, Birth Defects Res., Part A **79**, 281 (2007).

[5] M. L. Power and J. Schulkin, *Birth Distress and Disease: Placenta-Brain Interactions* (Cambridge University Press, Cambridge, 2005).

[6] D. J. Barker, Br. Med. J. **311**, 171 (1995).

[7] D. J. P. Barker, *Mothers, Babies and Health in Later Life*, 2nd ed. (Churchill Livingstone, Edinburgh, 1998).

[8] *The Placenta: From Development to Disease*, edited by H. H. Kay, D. M. Nelson, and Y. Wang (Wiley-Blackwell, Chichester, 2011), pp. 3–15.

[9] *The National Children's Study 2014: An Assessment. Panel on the Design of the National Children's Study and Implications for the Generalizability of Results; Committee on National Statistics; Division of Behavioral and Social Sciences and Education; Board on Children, Youth, and Families; National Research Council; Institute of Medicine*, edited by G. J. Duncan, N. J. Kirkendall, and C. F. Citro (National Academies Press, Washington, D. C., 2014). More information may be found at www.nichd.nih.gov/research/NCS.

[10] C. J. Newschaffer, L. A. Croen, M. D. Fallin, I. Hertz-Picciotto, D. V. Nguyen, N. L. Lee, C. A. Berry, H. Farzadegan, H. N. Hess, R. J. Landa, S. E. Levy, M. L. Massolo, S. C. Meyerer, S. M. Mohammed, M. C. Oliver, S. Ozonoff, J. Pandey, A. Schroeder, and K. M. Shedd-Wise, J. Neurodev. Disord. **4**, 7 (2012). More information may be found at www.earlistudy.org.

[11] A. Okabe, B. Boots, K. Sugihara, and S. N. Chiu, *Spatial Tessellations: Concepts and Applications of Voronoi Diagrams*. 2nd ed. (Wiley, Chichester, UK, 2000).

[12] D. Weaire, J. P. Kermode, and J. Wejcher, Philos. Mag. **53**, L101 (1986).

[13] P. A. Mulheran and J. A. Blackman, Philos. Mag. **72**, 55 (1995).

[14] J.-S. Ferenc and Z. Néda, Physica A **385**, 518 (2007).

[15] R. G. Shah, C. M. Salafia, T. Girardi, L. Conrad, K. Keaty, and A. Bartleotc *et al.*, Placenta **36**, 944 (2015).

[16] H. E. Stanley, Rev. Mod. Phys. **71**, S358 (1999).

[17] A. L. Koch, J. Theor. Biol. **12**, 266 (1966); **23**, 251 (1969).

[18] E. Limpert, W. A. Stahel, and M. Abbt, BioScience **51**, 341 (2001).

[19] R. L. Wasserstein and N. A. Lazar, Am. Statist. **70**, 129 (2016).

[20] T. W. Anderson and D. A. Darling, Ann. Math. Statist. **23**, 193 (1952).

[21] A. J. Arroyo and V. D. Winn, Semin. Perinatol. **32**, 172 (2008).

[22] D. S. Charnock-Jones, P. Kaufmann, and T. M. Mayhew, Placenta **25**, 103 (2004).

[23] *Autism Spectrum Disorders*, edited by D. Amaral, D. Geschwind, and G. Dawson (Oxford University Press, Oxford, 2011).

[24] P. Ch. Ivanov, M. G. Rosenblum, C.-K. Peng, J. Mietus, S. Havlin, H. E. Stanley, and A. K. Goldberger, Nature (London) **383**, 323 (1996).

[25] L. Cai, N. Friedman, and X. S. Xie, Nature(London) **440**, 358 (2006).

[26] S. A. Frank, J. Evol. Biol. **22**, 1563 (2009).

[27] H. Kurz, K. Sandau, J. Wilting, and B. Christ, in *Vascular Morphogenesis: In Vivo, In Vitro, In Mente*, edited by C. D. Little, V. Mironov, and E. H. Sage (Birkhauser, Boston, 1998), pp. 189–203.

[28] W. S. Kendal, Proc. Natl. Acad. Sci. USA **98**, 837 (2001).

[29] R. Karch, F. Neumann, M. Neumann, P. Szawlowski, and W. Schreiner, Ann. Biomed. Eng. **31**, 548 (2003).

[30] J. W. Evans, P. A. Thiel, and M. C. Bartelt, Surf. Sci. Rep. **61**, 1 (2006).

[31] D. L. Bergman and U. Ullberg, J. Theor. Biol. **193**, 171 (1998).

[32] D. H. Pretorius, T. R. Nelson, R. N. Baergen, E. Pai, and C. Cantrell, Ultrasound Obstet. Gynecol. **12**, 45 (1998).

[33] N. Schwartz, D. Mandel, O. Shlakhter, J. Coletta, C. Pessel, I. E. Timor-Tritsch, and C. M. Salafia, J. Ultrasound Med. **30**, 1171 (2011).

[34] M. Y. Rennie, J. G. Sled, and S. L. Adamson, Microcirculation **21**, 48 (2014).